

DRAFT

The packing fraction and dilution factor in RSS

Oscar A. Rondon, INPP - UVA

1 The dilution factor

The experimental asymmetry is formed from the difference over the sum of measured rates, or yields, of all the materials in the target. Following the derivation given in RSS TN# 2005-01 *The ^{15}N correction to the measured asymmetries*, we have

$$\varepsilon = \frac{L - R}{L + R} = \frac{P_b(N_{15}\sigma_{p(15)}A_{p(15)}P_{15} + N_1\sigma_1A_1P_1)}{N_{15}\sigma_{15} + N_1\sigma_1 + \sum N_A\sigma_A} \quad (1)$$

where N_A are the numbers of scattering nuclei of mass number A , $\sigma_A(W)$ represent radiated polarized $e - nucleus$ cross sections, P_b is the beam polarization and P_A is the polarization of nucleus A . The difference of polarized nucleon cross sections $\sigma_{p(A)}^L - \sigma_{p(A)}^R$ in the numerator has been expressed in terms of unpolarized nucleon cross sections $\sigma_{p(A)}$ and nucleon asymmetries $A_{p(A)}(W)$ (simplifying the subscript $p(1)$ to 1).

The customary approach is to factor out the product $N_1\sigma_1$ and write ε in terms of the proton dilution factor f_1

$$\varepsilon = f_1 P_b \left(\frac{N_{15}\sigma_{p(15)}}{N_1\sigma_1} A_{p(15)} P_{15} + A_p P_1 \right)$$

$$f_1 = \frac{N_1\sigma_1}{N_{15}\sigma_{15} + N_1\sigma_1 + \sum N_A\sigma_A} \quad (2)$$

The denominator of the dilution factor can be written in terms of the relative volume ratio of ammonia to LHe in the target cell, or packing fraction pf . For a cylindrical geometry, the packing fraction is exactly equivalent to the fraction of the cell's length that would be filled with ammonia.

Writing N_A in detail, $N_A = N_0\rho_A z_A/M_A$, where $N_0 = \text{Avogadro's number}$, ρ_A is the density of nuclear material A , M_A is the corresponding atomic or

molecular weight, and z_A is the thickness of the material, the dilution factor becomes ($f_1 \equiv f$)

$$f = \frac{\frac{3\rho_{NH_3}z_{NH_3}}{M_{NH_3}}\sigma_1}{\frac{3\rho_{NH_3}z_{NH_3}}{M_{NH_3}}\sigma_1 + \frac{\rho_{NH_3}z_{NH_3}}{M_{NH_3}}\sigma_{15} + \frac{\rho_{He}z_{He}}{M_{He}}\sigma_4 + \frac{\rho_{He}z'_{He}}{M_{He}}\sigma_4 + \frac{\rho_{Al}z_{Al}}{M_{Al}}\sigma_{27}} \quad (3)$$

where z_{He} represents LHe in the cell and z'_{He} is the external LHe (1 cm). z_{Al} represents the contributions of all the target walls in the view of the HMS acceptance \mathcal{A}_{HMS} . To simplify notation, we replace the subindices by the respective atomic or molecular weights. Using the known 3 cm cell length, the ammonia thickness is $z_{NH_3} = 3 pf$ cm, and

$$\begin{aligned} f &= \frac{\frac{3\rho_{18}3pf}{M_{18}}\sigma_1}{\frac{3\rho_{18}3pf}{M_{18}}\sigma_1 + \frac{\rho_{18}3pf}{M_{18}}\sigma_{15} + \frac{\rho_4 3(1-pf)}{M_4}\sigma_4 + \frac{\rho_4 z'_4}{M_4}\sigma_4 + \frac{\rho_{27}z_{27}}{M_{27}}\sigma_{27}} \\ &= \frac{\frac{3\rho_{18}}{M_{18}}\sigma_1}{\frac{3\rho_{18}}{M_{18}}\sigma_1 + \frac{\rho_{18}}{M_{18}}\sigma_{15} + \frac{\rho_4}{M_4}\left(\frac{1}{pf} - 1\right)\sigma_4 + \frac{\rho_4 z'_4}{M_4 3pf}\sigma_4 + \frac{\rho_{27}z_{27}}{M_{27} 3pf}\sigma_{27}} \\ &= \frac{3}{3 + \frac{\sigma_{15}}{\sigma_1} + \frac{\rho_4 M_{18}}{\rho_{18} M_4}\left(\frac{1}{pf} - 1\right)\frac{\sigma_4}{\sigma_1} + \frac{\rho_4 M_{18} z'_4}{\rho_{18} M_4 3pf}\frac{\sigma_4}{\sigma_1} + \frac{\rho_{27} M_{18} z_{27}}{\rho_{18} M_{27} 3pf}\frac{\sigma_{27}}{\sigma_1}} \end{aligned} \quad (4)$$

All quantities in the above expression are universal or experimentally measured ones ($z'_4 = 1$ cm and $z_{27} = 0.03$ cm,) except pf , which is not measured geometrically and is specific to each of *RSS*'s target cells¹. Collecting first the He terms, and replacing next the well known values for the lengths, densities and masses (see <http://www.jlab.org/~jones/rss/rsstgt.htm>).

$$f = \frac{3}{3 + \frac{\sigma_{15}}{\sigma_1} + \frac{\rho_4 M_{18}}{\rho_{18} M_4}\left(\left(\frac{1}{pf} - 1\right) + \frac{z'_4}{3pf}\right)\frac{\sigma_4}{\sigma_1} + \frac{\rho_{27} M_{18} z_{27}}{\rho_{18} M_{27} 3pf}\frac{\sigma_{27}}{\sigma_1}}$$

¹The tiny contribution of the proton NMR coils, which can be included at any time for a more accurate form, is neglected here.

$$= \frac{3}{3 + \frac{\sigma_{15}}{\sigma_1} + 0.7112\left(\frac{4}{3pf} - 1\right)\frac{\sigma_4}{\sigma_1} + \frac{0.022}{pf}\frac{\sigma_{27}}{\sigma_1}} \quad (5)$$

For $pf = 0.5$, the dilution factor is

$$f = \frac{3}{3 + \frac{\sigma_{15}}{\sigma_1} + 1.185\frac{\sigma_4}{\sigma_1} + 0.044\frac{\sigma_{27}}{\sigma_1}} \quad (6)$$

In DIS, $\sigma_A \sim A\sigma_1$, so

$$f(pf = 0.5) = \frac{3}{3 + 15 + 1.185 \times 4 + 0.044 \times 27} = \frac{3}{3 + 15 + 4.74 + 0.59} \quad (7)$$

which shows that He and Al contribute about 23% of the dilution. In the resonances, the ratio $\sigma_n/\sigma_p < 1$, and the contributions of He and Al decrease, but they are still about 15 to 18%, depending on pf .

For a pure ammonia target, the dilution factor is $f = 1/(1 + \sigma_{15}/(3\sigma_1))$, which can be crudely approximated by $f = 1/(3.33 + 2.67\sigma_n/\sigma_1)$, where σ_n is the neutron cross-section per nucleon in nuclei, σ_1 is the free proton cross section, and we took the proton cross section in nuclei as $\sigma_p \simeq \sigma_1$. This approximation is reasonable in DIS, but is inaccurate in the resonances.

2 Finding the packing fraction

From the first equality in eq.(4) we see that the denominator of the dilution factor (which actually is just the total yield, or rate, Y_T , that depends on the beam charge or current I_b and the HMS acceptance \mathcal{A}_{HMS} , before these two factors cancel out with the corresponding ones in the numerator) can be written as a linear function of the packing fraction:

$$\begin{aligned} Y_T &= I_b \mathcal{A}_{HMS} \left(\frac{\rho_{18}}{M_{18}} 3pf(3\sigma_1 + \sigma_{15}) + \frac{\rho_4 3(1 - pf)}{M_4} \sigma_4 + \frac{\rho_4 z'_4}{M_4} \sigma_4 + \frac{\rho_{27} z_{27}}{M_{27}} \sigma_{27} \right) \\ &= I_b \mathcal{A}_{HMS} \left(\left(\frac{\rho_{18}}{M_{18}} (3\sigma_1 + \sigma_{15}) - \frac{\rho_4}{M_4} \sigma_4 \right) 3pf + \frac{\rho_4}{M_4} (3 + z'_4) \sigma_4 + \frac{\rho_{27} z_{27}}{M_{27}} \sigma_{27} \right) \\ &= m pf + b \end{aligned} \quad (8)$$

where the slope m and intercept b are given by (with $z'_4 = 1$)

$$\begin{aligned} m &= 3I_b \mathcal{A}_{HMS} \left(\frac{\rho_{18}}{M_{18}} (3\sigma_1 + \sigma_{15}) - \frac{\rho_4}{M_4} \sigma_4 \right) \\ b &= I_b \mathcal{A}_{HMS} \left(4 \frac{\rho_4}{M_4} \sigma_4 + \frac{\rho_{27} z_{27}}{M_{27}} \sigma_{27} \right) \end{aligned} \quad (9)$$

This linear form allows us to calculate the packing fraction pf^* of the data by interpolating the actual data yield $Y_T^*(pf^*)$ between two values of simulated $Y_T(pf_i)$ corresponding to two values $pf_{i=1,2}$ of the packing fraction near the expected pf^* .

As expected, the intercept b depends exclusively on the rate from LHe and the window material. The factor of 4 corresponds to the 3 cm target cell length filled only with LHe for $pf = 0$, plus 1 cm of LHe outside the cell. Therefore, to good accuracy, b can be determined independently by comparing data and Montecarlo (MC) rates for empty cell runs with LHe. The accuracy is limited by the absence of cell lids and NMR coil in the empty cell, which is partly compensated by the rate from the tungsten wire cross hairs. This difference could limit the accuracy to a few percent.

The simulated yields may need to be scaled by some factor s to get agreement between the simulation and the data's yield for the LHe filled empty cell, or with a target of known thickness $z_C = z_C$, such as the C disks

$$\frac{Y_C^*}{Y_C} = \frac{I_b^* \mathcal{A}_{HMS}^* z_C^* \sigma_C^*}{I_b \mathcal{A}_{HMS} z_C \sigma_C} = \frac{I_b^* \mathcal{A}_{HMS}^* \sigma_C^*}{I_b \mathcal{A}_{HMS} \sigma_C} = s. \quad (10)$$

$s = 1$ for perfect data and MC agreement. If the simulation's model cross section is well known at the kinematics of the measurement, the ratio reduces to a scale factor between simulated $I\mathcal{A}$ and actual $I^*\mathcal{A}^*$ products. The simulated yields $Y_T(pf_i)$ will scale, but not on a parallel line: the change in the slope m to $m' = sm$ may increase or decrease the sensitivity of pf^* to the simulated yields: if $s > 1$, the data's packing fraction will be less sensitive to the simulation, and vice versa.

If the cross section is not well known, the scale factor is ambiguous with respect to either $I\mathcal{A}$ or the cross section. In the assumption that the former are better known, the scale factor would apply to the He or C cross section and, in the QFS model, to the other nuclear cross sections too. The intercept b' scales as $b' = sb$ independently of the quantity to which the scale is applied but the slope scales differently, if the nuclear cross sections are scaled, instead

of IA , because the free proton cross section σ_1 remains unchanged

$$\begin{aligned}
 m'' &= 3I_b \mathcal{A}_{HMS} \left(\frac{\rho_{18}}{M_{18}} (3\sigma_1 + s\sigma_{15}) - \frac{\rho_4}{M_4} s\sigma_4 \right) \\
 &= m' + 3I_b \mathcal{A}_{HMS} \frac{\rho_{18}}{M_{18}} 3\sigma_1 (1 - s).
 \end{aligned}
 \tag{11}$$

From eq.(5) it can be seen that scaling the current times acceptance product does not affect the ratios of proton to nuclear cross sections in the dilution factor, while scaling the nuclear cross sections does.

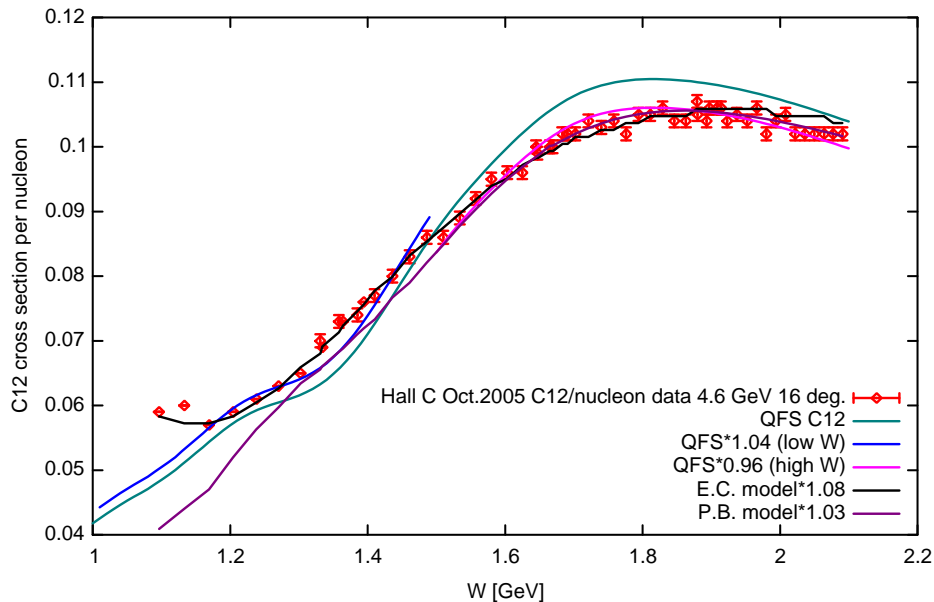


Figure 1: Hall C 4.6 GeV preliminary ^{12}C data and models.

The recent availability of nuclear cross sections at kinematics similar to those of RSS , makes it possible to separate adjustments to the model cross sections from the scale factors that apply to the IA product only. As shown on Figures 1 and 2, the QFS model agrees with preliminary Hall C data at the $<6\%$ level. This level of agreement allows the choice of scaling only the IA product, leaving the nuclear cross sections unchanged, or adjusting the cross sections for best agreement with data and using improved data/MC ratios for C.

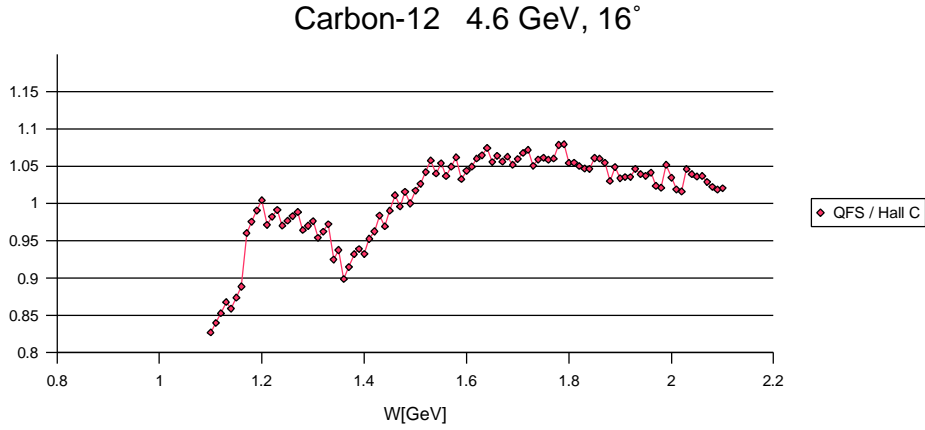


Figure 2: Ratio QFS/Hall C 4.6 GeV data.

The procedure to get the packing fraction and dilution factor would be as follows:

- get scale factors for high and low momenta comparing Montecarlo to data yields for C. We have those factors already, but we may want to update them, by using a better model for C, or by correcting QFS with the ratio of QFS to Hall C data (see Figure 1 and 2). Since the acceptance when the target magnetic field is ON may depend on the HMS central momentum setting (due to the momentum dependence of the particle trajectories before they enter the HMS), separate scale factors may be needed.
- calculate Montecarlo yields $Y_T(pf = 0.5)$, $Y_T(0.6)$. Scale the yields by the factors found previously to convert them to equivalent data yields $Y_T^*(0.5)$, $Y_T^*(0.6)$. Alternatively, solve for m and b and scale them.
- solve for pf^* using the data's total yield Y_T^* , by comparing to the simulated scaled yields, or using m and b as discussed in the next sections.
- apply pf^* to the Montecarlo to get the dilution factor from the ratio of proton to total radiated yields.

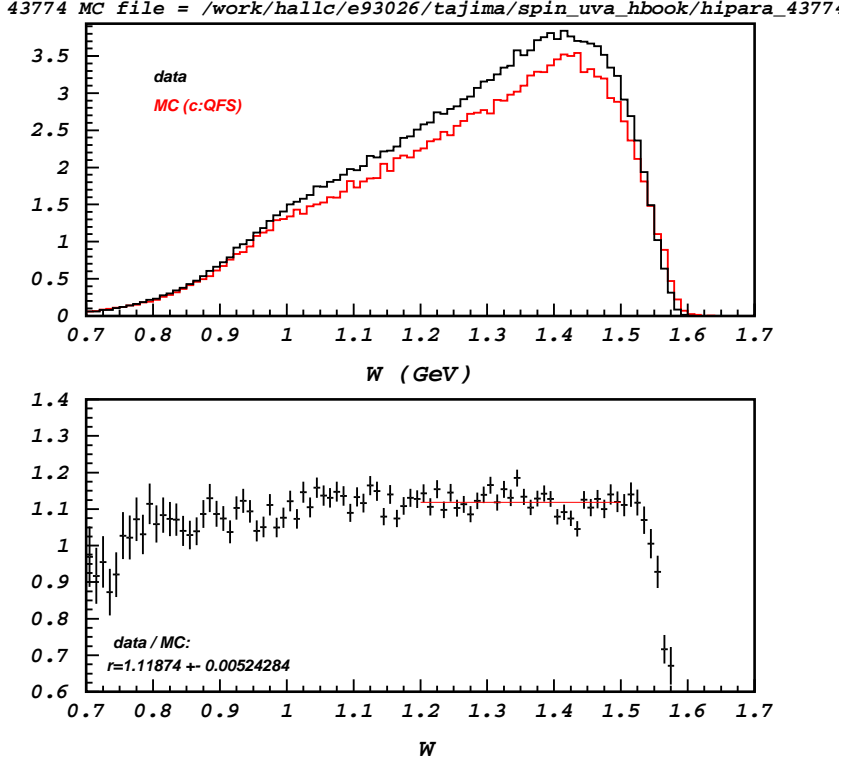


Figure 3: Parallel data and MC yields for C disk targets (top) and data/MC ratio, high HMS p .

3 Error propagation

In terms of the data's Y_T^* , the packing fraction is

$$pf^* = \frac{Y_T^* - b}{m} \quad (12)$$

which shows that pf^* should be independent of the current and acceptance, if the calculated slope and intercept reflect the actual values corresponding to the data. If the actual and simulated products $I^* \mathcal{A}^* / (IA) = s$

$$pf^{*'} = \frac{Y_T^* - b'}{m'} = \frac{Y_T^* - sb}{sm} \quad (13)$$

and the error on pf^* due to s is

$$dpf^* = -\frac{Y_T^*}{s^2 m} ds = -\frac{Y_T^*}{m'} \frac{ds}{s} \quad (14)$$

The fractional change in pf^* can be magnified relative to the change in scale factor, according to eq. (14). As we show in the next section, the scale factor in RSS is always > 1 , so actually the error δs is reduced somewhat when propagated to δpf^*

The uncertainty due to the input models can be treated separately, by comparing the models to data, and calculating the propagation of the models' errors to m and b .

The statistical error in pf^* comes from dY_T^* .

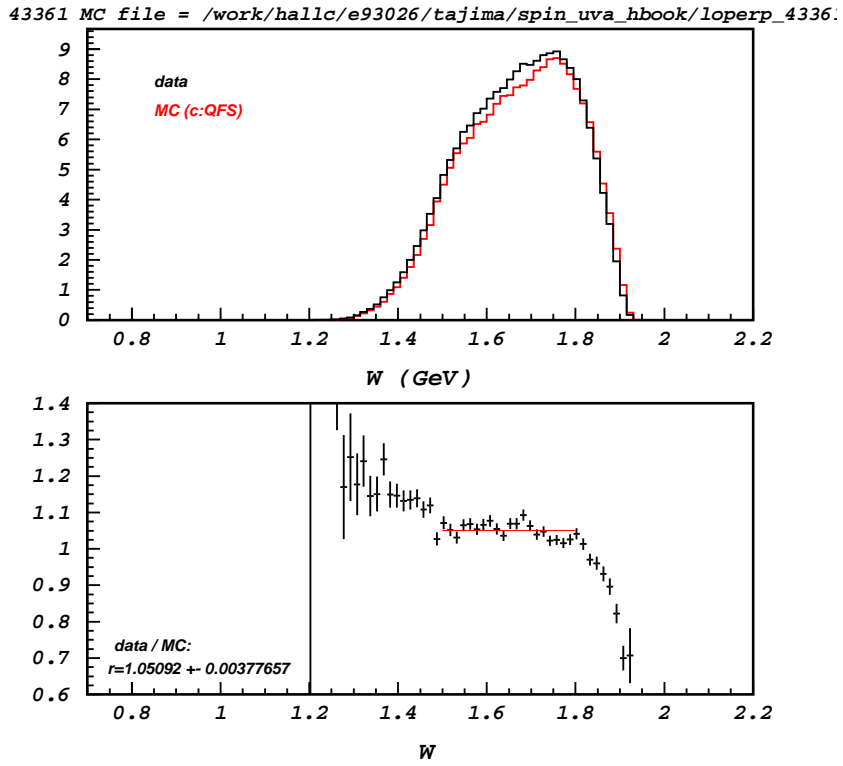


Figure 4: Perpendicular data and MC yields for C disk targets (top) and data/MC ratio, low HMS p .

4 Numerical examples

The procedure described above has been applied to the RSS data. Some important observations can be made when examining the results:

- a constant data/MC yield ratio as a function of W is an indication that the shape of the model cross sections reproduce well the data, although data and MC may differ by a normalization factor. Figures 3 and 4 illustrate this ratio for the C disk targets for parallel data at high HMS momentum p setting and for perpendicular low momentum data, respectively. Since the pf is independent of kinematics, integrating the yields over the W ranges where the data/MC ratio is flat improves the precision.

- there are two different sets of rates, corresponding to the very different average cross sections for the high and low p settings. Table 1 shows the parallel data and MC yields integrated over $1.2 \text{ GeV} < W < 1.5 \text{ GeV}$ for high p and $1.5 \text{ GeV} < W < 1.8 \text{ GeV}$ for low p , and the resulting slopes and intercepts with (pf^{*} , last column,) and without (pf^{*}) application of the data/MC scale factors determined from the C yield ratios (column 3). The first three rows correspond to the MC yields calculated with the unmodified QFS cross section for ^{12}C . The average pf 's are in **bold**. The second set of

TABLE 1

	Scalein	C target data/MC	Y* (data)	Y MC (50%)	Y MC (60%)	m	b	pf*	m'	b'	pf*'
High p	1.000	1.119	126.8	107.1	119.3	122.0	46.2	0.661	136.5	51.6	0.551
Low p	1.000	1.049	236.9	222.2	246.0	237.7	103.4	0.562	249.4	108.4	0.515
								0.611			0.533
High p	1.040	1.084	126.8	110.0	122.5	124.5	47.8	0.635	134.9	51.8	0.556
Low p	0.960	1.090	236.9	215.1	238.2	231.5	99.3	0.594	252.4	108.2	0.510
								0.615			0.533
High p	1.040	1.106	126.8	110.0	122.5	124.5	47.8	0.635	137.6	52.8	0.537
Low p	0.960	1.069	236.9	215.1	238.2	231.5	99.3	0.594	247.4	106.1	0.529
								0.615			0.533

three rows are the results for the QFS model scaled with the “scalein” factor adjusted to agree with the recent Hall C data shown in Figure 1². It can be seen that although the high and low momentum pf^{*} are different, the average is insensitive to either the QFS scale or the C data/MC scale. The last three rows show the effect of arbitrarily changing the C data/MC scale

²The “scalein” factors applied to the model Born cross section in QFS also improve the agreement between the high and low p C data/MC ratios, which is an indication that the residual scale factors are due to the IA product, rather than the model. Improvement is also seen for the perp data, see Table 2, 2nd. row

by +2% (high p) and -2% (low p). The pf^{*} for low and high p become much more similar with just small changes in the scale factor.

- the slopes and intercepts are correspondingly different for each momentum setting. Since the data yields Y_T^* are also different, the pf determined for each momentum setting is an independent measurement. Fig. 5 shows the resulting sets of $Y(pf) = m pf + b$ yield lines for the top 6 rows of Table 1. Note that because the respective scaled m' and b' are almost identical, the lines for rows 1 and 4, or 2 and 5, lie almost on top of each other. The intersections of the lines of constant integrated data Y_T^* for high and low momentum with the $Y(pf)$ lines give in graphical form the pf^{*} measured for each case. It can be seen that the data lines would have to intercept the $Y(pf)$ lines exactly on top of each other to result in identical pf^{*} 's, but even small errors in either m or b can result in different values. However, as with any set of independent measurements of the same quantity, taking the average provides a more reliable result than any individual measurement.

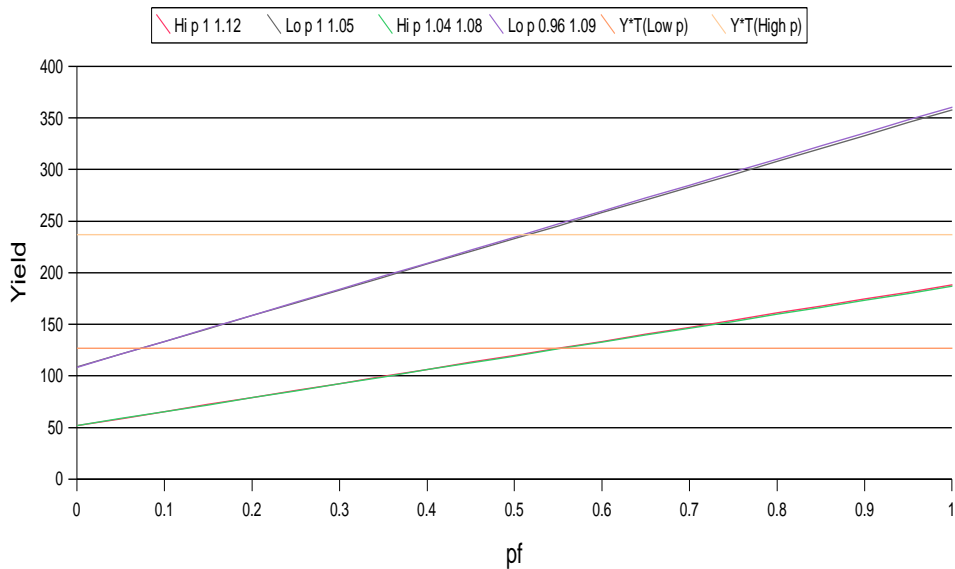


Figure 5: Yields vs packing fraction, high and low momentum settings.

- the average of the low and high momentum packing fractions is rather insensitive to the individual variations, if they are the result of random errors in m and b . On the other hand, correlated changes on the high and low momentum scale factors can systematically shift the average. However,

it is such shifts that give rise to the non-unity data/MC ratios in the first place, so applying the scale factors based on the C ratios effectively takes care of the systematic corrections due to current and acceptance. The remaining uncertainties, such as those due to the model cross sections, are random fluctuations about the true cross section value. This is illustrated by the near constancy of the average pf 's for all configurations and several choices of cross section models and resulting C data/MC scale factors detailed in S. Tajima's dilution factors URL: <http://www.jlab.org/tajima/rss/>, which are summarized in Table 2.

TABLE 2

Model	scalein		Parallel				Perp			
	high p	low p	C data/MC		Average pf^{*} '		C data/MC		Average pf^{*} '	
			high p	low p	Top	Bottom	high p	low p	Top	Bottom
QFS 12/05	1	1	1.119	1.049	53.4	54.3	1.094	1.051	57.5	60.2
"	0.96	1.04	1.084	1.090	53.4	54.2	1.060	1.092	57.3	59.9
QFS < 12/05	1	1	1.119	1.049	53.3	54.3	1.107	1.085	57.3	59.5
P. Bosted	-	-	1.171	1.153	53.9	54.6	1.159	1.200	58.0	60.2
QFS 10/05	1.11	1.07	1.037	0.983	54.2	54.6	1.034	1.017	57.9	60.4

- additional measurements of the packing fraction can be obtained by using data at other HMS momentum settings, such as the runs taken with very high $p_0 = 4.96$ GeV, and can be averaged with the high and low p , for improved precision.

- since the QFS model agrees well with the abundant quasielastic data, the error due to the model can be further reduced by comparing both C and ammonia data to MC in the region $W < 900$ MeV. Figures 6 and 7 illustrate the low energy loss ν side of the quasielastic region for ${}^4\text{He}$ at 4.3 GeV, 15° and ${}^{12}\text{C}$ at 3.6 GeV, 20° .

In summary, although not all forms of obtaining the pf have been exhausted in our analysis, we can be confident that the values we are using are well understood.

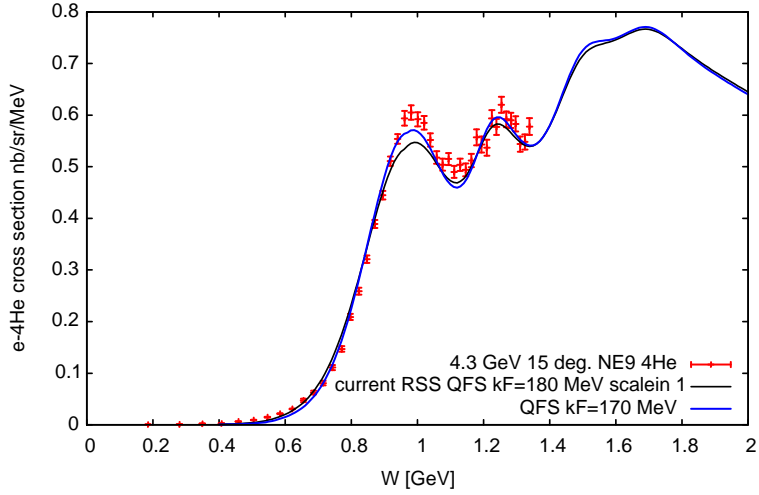


Figure 6: ${}^4\text{He}$ cross section at 4.3 GeV and 15° from SLAC NE-9 and QFS model. The current Fermi momentum $k_F = 180$ MeV was applied to smooth the model to match the data for $W > 1.1$ GeV, although $k_F = 170$ MeV works better in the quasielastic region.

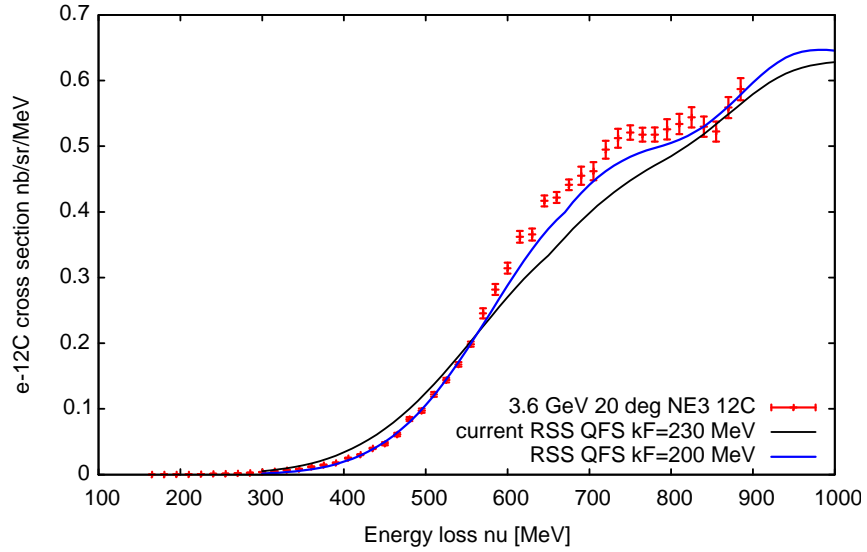


Figure 7: ${}^{12}\text{C}$ cross section at 3.595 GeV and 20° from SLAC NE-3 and QFS model. As for ${}^4\text{He}$, a larger value of $k_F = 230$ MeV gives better agreement in the inelastic region (see Figure 3).

APPENDIX

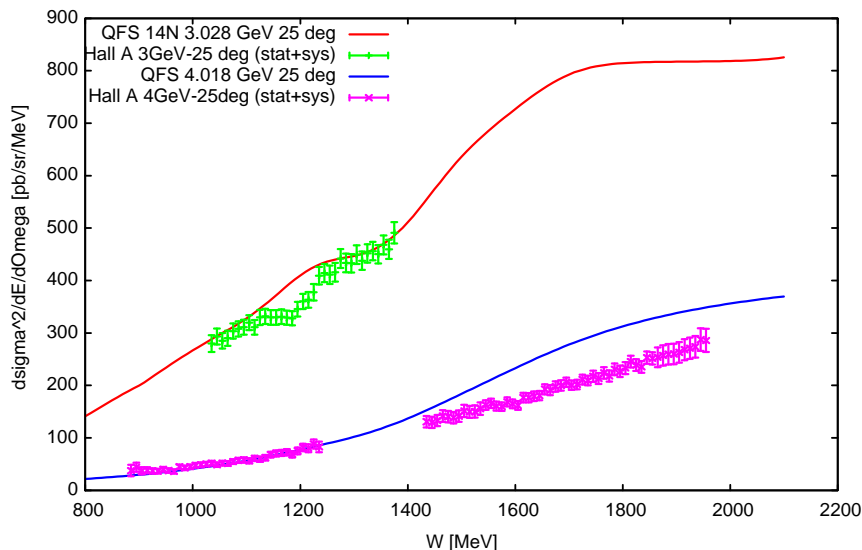


Figure 8: Preliminary ^{14}N cross section at 4.02 GeV, 25° and 3.03 GeV, 25° from Hall A and QFS model. Statistical and systematic errors added in quadrature. Kind courtesy of P. Solvignon – Not for publication.

Figure 8 shows a comparison between recent preliminary ^{14}N cross section data from JLab Hall A and QFS, at 4.018 GeV, 25° and 3.028 GeV, 25° . These data sets were chosen because they are closest to *RSS* kinematics, see Figure 9. These results, combined with those of Figure 2 show that QFS agrees well in shape with data at kinematics near that of *RSS* for $\sim 1.1 \text{ GeV} < W < \sim 1.5 \text{ GeV}$ with little or no need for a normalization factor. Above $W = 1.5 \text{ GeV}$, a normalization (“scalein”) factor of ~ 0.96 gives good agreement.

The purpose of this comparison is to show that the systematic error in the dilution factor f due to the model Born cross sections for $A > 2$ is about 2% relative for $W < 1.5 \text{ GeV}$ and 4% or less for higher W , since f depends mainly on the ratios of the Born cross sections for N and He to protons and deuterons (radiative corrections play also a limited role, since the ratios are for radiated cross sections).

The elementary cross sections that make up the inclusive QFS cross section are shown on Figure 10, along with the Hall A 4 GeV 25° data. The

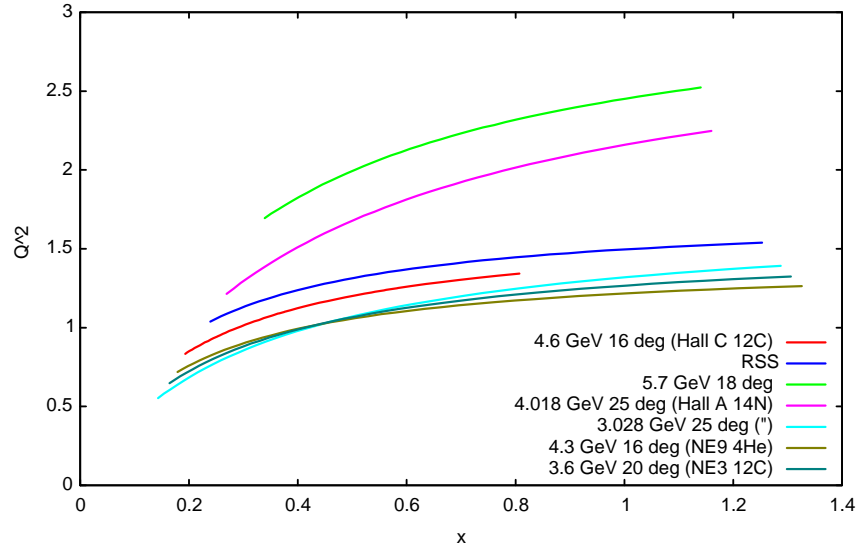


Figure 9: Central kinematics of data used in comparisons to QFS. Some curves may extend beyond the actual regions containing data and are plotted only to display the relation between the *RSS* kinematics and other experiments mentioned in the text.

DIS part is the dominant component, and the effect of reducing one of its amplitudes by a factor of 0.8 is shown as “test QFS”. However, applying this factor may not work with the *RSS* data for the C disk target at 3.6 GeV beam energy and no target field, which showed the best agreement with the MC. The Hall A version of QFS is also plotted.

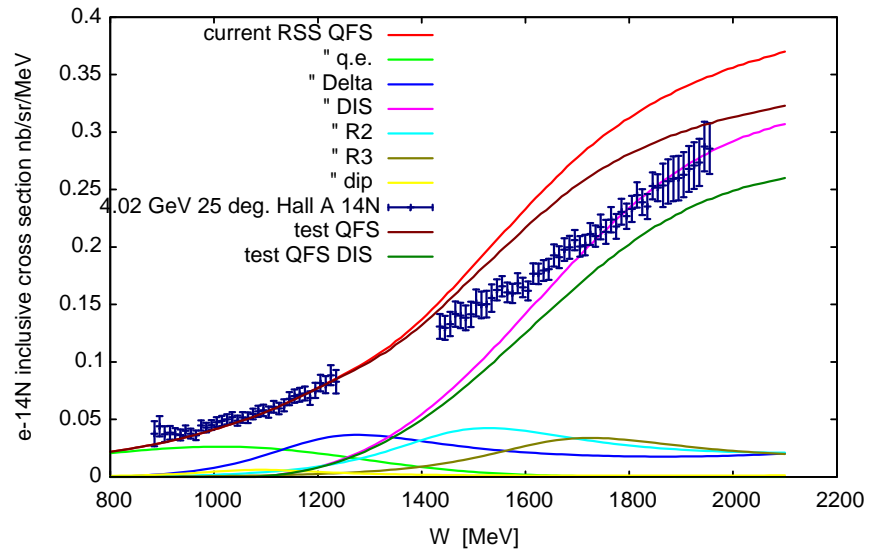


Figure 10: Preliminary ^{14}N cross section at 4.02 GeV, 25° from Hall A and QFS model components. Also plotted are a test example of reducing one of QFS's DIS components by 0.8 – Not for publication.